Reversal of current blockade in nanotube-based field effect transistors through multiple trap correlations

Jack Chan,[1] Brian Burke,[1] Kenneth Evans,[1] Keith A. Williams,[1,*] Smitha Vasudevan,[2] Mingguo Liu,[2] Joe Campbell,[2] and Avik W. Ghosh[2]

[1]*Department of Physics, University of Virginia, Charlottesville, Virginia 22904, USA*

[2]*Department of Electrical and Computer Engineering, University of Virginia, Charlottesville, Virginia 22904, USA*

(Received 31 December 2008; revised manuscript received 8 May 2009; published 1 July 2009)

Current noise in electronic devices usually arises from uncorrelated charging events, with discrete transitions resolved only at low temperatures. However, in nanotube-based field effect transistors (FETs), we have observed random telegraph signal (RTS) with unprecedented amplitude *at room temperature*. This RTS is characteristically truncated, suggesting that the current blockade induced by one trap *fully reverses* through electrostatic interaction with another. These observations have motivated us to develop a robust quantum transport model that reveals how the fast varying, logarithmic gate potential along a one-dimensional channel makes it possible to detect correlated transitions arising from multiple charge traps. These results suggest applications including adsorbate detection and spectroscopy and the development of strategies to passivate traps and mitigate current noise in FETs.

DOI: 10.1103/PhysRevB.80.033402 PACS number(s): 85.35.−p, 61.48.De, 85.30.Tv

As a consequence of miniaturization, transistor channels acquire a larger surface-to-volume ratio and become increasingly susceptible to stochastic effects, e.g., random telegraph signals (RTSs) and $1/f$ noise arising from dopant fluctuations, dangling bonds, and charge traps at surfaces and interfaces. In bulk Si- metal-oxide-semiconductor field effect transistors (MOSFETs), RTS has been studied for several decades,[1] but it is typically seen only at temperatures of a few kelvin. One-dimensional quantum confinement amplifies the effects of individual defects through enhanced wavefunction overlap with carriers; hence, RTS can be well resolved at high temperatures in nanotube-based transistors.[2,3] In this paper, we show that enhanced trap-channel interaction and the logarithmic electrostatic potential around the 1D nanotube channel lead to the observation of correlated, multiple-trap RTS that is clearly resolved even at room temperature.

The fabrication process of a typical carbon nanotube (CNT)-FET inevitably introduces defects on the CNT, in the oxide, or at their interfaces[4] through the high-temperature annealing of SiO_2 in H_2 (Ref. 5) and the interaction with high-energy electrons from electron-beam microscopy.[6] This report focuses on RTS observed in long-channel (20 μm) nanotube FETs in which scattering effects are most readily obtained. Defects along the channel can trap charges, which may subsequently interact electrostatically with carriers; the stochastic trapping and detrapping of carriers near resonance with the Fermi level E_F create a flicker in the output current in the form of RTS.[7–10] Our RTS data (Fig. 1) are unique in several important aspects: (a) the RTS amplitude reaches 80% of the baseline ambipolar current, even at room temperature [Fig. 1(a)]; (b) a characteristically truncated, gateable Coulomb blockade window, flanked by RTS on either side, indicates near-complete blocking and subsequent unblocking of conduction [Fig. 1(b)]; and (c) our observations are consistent with a quantum transport model [Figs. 1(c) and 1(d)] for current flow coupled with a self-consistent Coulomb potential for multiple-trap interaction and a Monte Carlo simulation of stochastic switching. This model clearly illustrates how the logarithmically varying capacitance of the nanotube (Fig. 3) allows a distant gate to tune the blockade and resolve the cooperative effects of two nearby traps that passivate each other to restore full current (Fig. 2).

Experiment. CNT-FETs were fabricated on B-doped Si(100) substrates with a 500-nm-thick thermal oxide and resistivity of 0.001–0.0025 $\Omega\,\mathrm{cm}^{-1}$ (SQI). Catalysts were deposited on prepatterned sites, and CNTs were grown on the oxide surface by chemical vapor deposition (CVD).[11] After annealing with H_2 at 900 °C for 10 min, CVD synthesis is carried out for 15 min using methane and hydrogen at the same temperature. Ti/Au electrodes were deposited by photolithography over selected isolated CNTs to introduce source and drain contacts after analysis by scanning electron microscopy. The contacts were then annealed in argon 99.999% (GT&S) at atmospheric pressure and at a temperature of 600 °C for 5 min.[12,13] As usual for these prototype devices, the conductance through the CNT channels is modulated by a universal backgate (doped poly-Si). With the device contained in a variable temperature probe station (TTP-4 Probe Station, Desert Cryogenics) and using a source meter (Keithley 2602), we measure the source-drain current (I_{ds}) as a function of the backgate voltage (V_{gs}) and source-drain bias (V_{ds}). Samples are typically kept under vacuum at 1×10^{-6} Torr for 24 h before measurement.

The focus of this report is the transport data presented in Fig. 1, which shows a pronounced, notchlike drop in current over a small bias window in the vicinity of the broader and smoother conductance dip typical of an ambipolar FET. The notch was found to shift reproducibly with bias V_{ds}. Closer examination reveals RTS arising from trapping and detrapping events on both sides of the notch. The RTS is robust and detectable for several days under vacuum with clearly resolved amplitude at room temperature. The RTS-mediated blockade window is observed in the electron conduction region (Fig. 1) but not for hole conduction (except a smaller notch with analogous gate-dependent shifts, which could be the remnants of a similar but narrower blockade window for hole conduction).

 ©2009 The American Physical Society

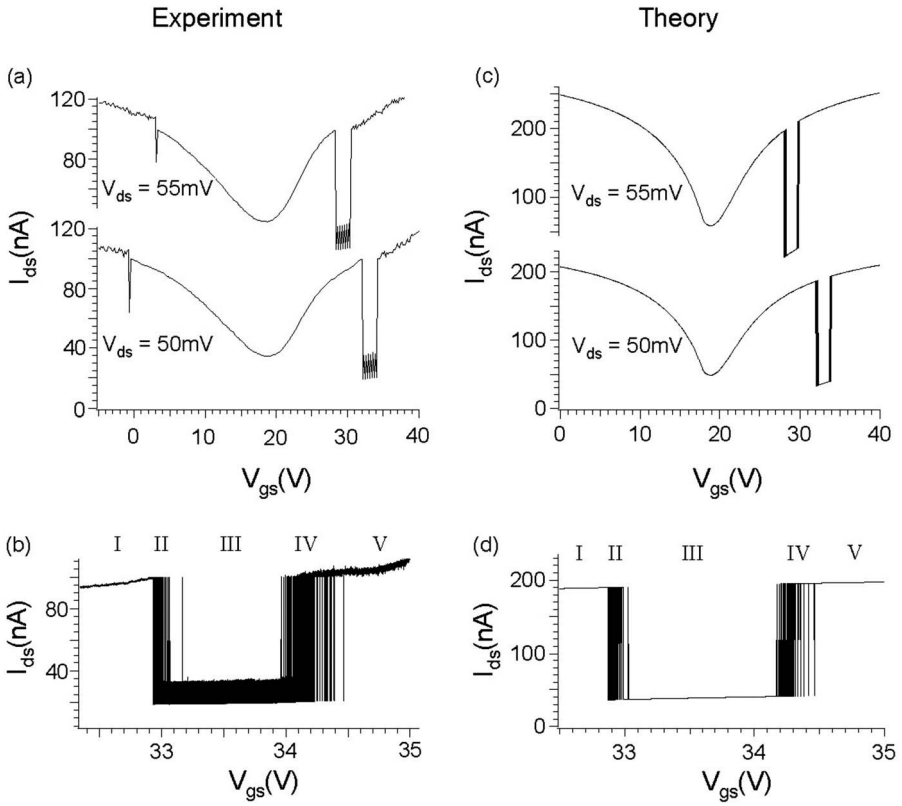

FIG. 1. (a) I_{ds}-V_{gs} plots for V_{ds}=50 and 55 mV, measured at room temperature under vacuum. Five different transport regimes are identified with numerals. Scan rate and scan resolution are 80 V/sec and 6.25 data points/V, respectively. (b) Higher-resolution scan of I_{ds} versus V_{gs} at the blockade window for V_{ds}=50 mV. Scan rate and scan resolution are 0.125 V/sec and 4000 data point/V, respectively. (c) and (d) NEGF simulation of current flow through CNT-FET coupled with Monte Carlo model for trap-assisted scattering. The physics in the different regimes of the *I-V* are spelt out in the spectral evolution diagram of Fig. 2 and the accompanying text

While RTS is not unexpected in this type of device, the amplitude at ambient temperature is very unusual, and truncated blockade with different RTS time constants strongly suggests a multiple-trap effect that is electronically correlated. This observation is consistent with a previous paper by Liu and Wang,[14] who presented statistical evidence for correlated RTS in nanotube-based transistors at low temperature.

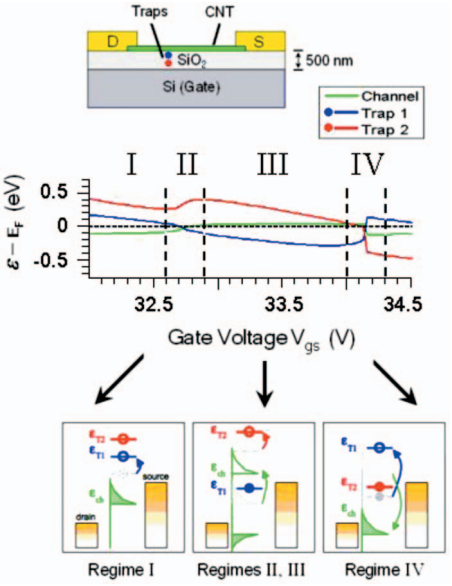

FIG. 2. (Color) (Top) Schematic diagram of CNT-FET with traps in SiO_2. (Center) Simulated evolution of trap levels and channel conduction band-edge under gate bias, influenced by self-consistent Coulomb repulsion. The sequence of energy level diagrams (below) shows the exchange of level positions under these repulsive forces. Expulsion of the channel from the conduction window (regimes II and III) blocks the current, while its reintroduction (regime IV) unblocks it.

Theory. Motivated by the truncated RTS evident in our data, the transfer characteristic (I_{ds}-V_{gs}) of a device was modeled using the nonequilibrium Green's function (NEGF) formalism[15] coupled with a Monte Carlo simulation of the stochastic trap dynamics near resonance.[16] As we establish later, the truncated blockade window likely arises from two traps sitting inside the oxide between the CNT channel and backgate. Each trap density of states (DOS) is modeled by a Lorentzian of the form $D_t(E)=\gamma_t/2\pi[(E-\epsilon_t)^2+(\gamma_t/2)^2]$, while the CNT DOS is given by $D_{ch}(E)=D_0|E|\Theta(|E|-E_g/2)/\sqrt{E^2-(E_g/2)^2+\eta}$.[17] $D_0=8/3\pi a_{cc}\gamma_0$ is the low-bias metallic CNT DOS (a_{cc} denotes the carbon bond length, γ_0 =2.5 eV is the nearest-neighbor overlap integral, E_g is the CNT band gap, η is a phenomenological dephasing parameter for incoherent scattering in the long tube, and Θ is the Heaviside step function). The DOS states are shifted by the interatomic potentials to compute the charge and current in the NEGF formalism. We calculate the number of electrons of the ith level (ch, T_1, and T_2, respectively, labeling the CNT channel, trap 1 and trap 2) by integrating its DOS with the weighted Fermi functions $f_{S,D}$ (S=Source; D=Drain). With contact-broadening parameters $\gamma_{S,i}$ and $\gamma_{D,i}$ we obtain

$$N_i = \int dE D_i(E-U_i)\left[\frac{\gamma_{S,i}f_S(E)+\gamma_{D,i}f_D(E)}{\gamma_{S,i}+\gamma_{D,i}}\right]. \quad (1)$$

We note that while NEGF models are widely used for computing current flow, getting the RTS-mediated blocking and

unblocking requires *self-consistency*, *stochasticity*, and most significantly *self-interaction correction*. The latter many-body problem, positing that a charge should not feel a potential due to itself, can be solved exactly for a few scattering ground states by introducing an explicit level-dependent potential. For example, the strongly correlated Coulomb potential acting on trap 1 is given by $U_{T1}=\Delta N_{ch}U_{0,T1-ch}+\Delta N_{T2}U_{0,T1-T2}$, where ΔN_i is the deviation in the ith level population from equilibrium and $U_{0,j-i}$ is the Coulomb interaction matrix between the ith and jth levels. These potentials are calculated self-consistently with the computed charges from Eq. (1) as all three levels are affected by each other. (We also need to invoke a sizeable Laplace asymmetry so that one trap can "passivate" another but not be passivated by it. This is provided by the logarithmic potential variation perpendicular to the CNT, generating widely different capacitive gate transfer factors α_g for the distinct trap energies that slip at different rates past each other). Finally, the converged channel potential yields the steady-state CNT current

$$I=\frac{2e}{h}\int dED_{ch}(E-U_{ch})\frac{\gamma_{S,ch}\gamma_{D,ch}}{\gamma_{S,ch}+\gamma_{D,ch}}[f_S(E)-f_D(E)] \quad (2)$$

In order to obtain the stochastic RTS signatures, the steady-state equations are modulated by the time-dependent trap potentials. These potentials become stochastic near the gate-tuned resonance between the trap's energy level and the CNT contact Fermi energies so that the occupancy of the traps becomes fractional. To simulate the stochastic trap dynamics, we set up a two-state Monte Carlo simulation that depends only on the trap capture time τ_c and emission time τ_e, relevant to a filled and an empty trap, respectively.[16] For a trap with energy ϵ_T in thermal equilibrium with its environment, detailed balance requires[18–21]

$$\frac{\tau_c}{\tau_e}=2\exp\left[\frac{-(\epsilon_T-E_F)+\alpha_g|e|(V_{gs}-V_{g0})}{k_BT}\right]. \quad (3)$$

The prefactor accounts for spin degeneracy, while V_{gs} is the gate voltage relative to the grounded source. V_{g0} is the value of the minimum in the ambipolar I_{ds}-V_{gs} curve, which corresponds to a gate offset[22] due to other distant traps that do not contribute to the dynamics of the RTS signals. We use a given scan rate to convert temporal noise into voltage noise.

Results. Figure 1 demonstrates a compelling reproduction of the experimental data by our simulation model (parameters listed in Ref. 23). While the detailed transition voltages and current jumps depend on these parameters, the overall physics of blocking and unblocking is robust with respect to parameter variations. Our only assumption is that the traps reside at different distances from the channel with a corresponding hierarchy of interaction strengths ($U_{0,T1-T2}>U_{0,T1-ch}>U_{0,T2-ch}$). The physics of the RTS-mediated blocking and unblocking can be understood by looking at the steady-state dynamics of the individual traps and channels computed by our model under their mutual self-consistent repulsion.

Figure 2 plots the gate-induced migration of the levels (the peak DOS of the traps and the conduction band-edge for the CNT) as extracted from their self-consistently computed steady-state potentials U_i. The levels slip at very different rates controlled by the Laplace part α_g of the potential, varying logarithmically with distance from the gate. A positive gate voltage pushes the levels down, filling them sequentially upon entering the conduction window between the source and drain electrochemical potentials. Filling the CNT conduction band (regime I) repels trap 1 mildly and barely influences trap 2 sitting further away. When the first trap is filled, it pushes the CNT out of the conduction window and starts the onset of blockade (regime II). This expulsion proceeds through an RTS sequence dictated by the steady-state occupancy of trap 1 [Eq. (3)], ending with a fully filled trap and a completely blocked channel (regime III). At this stage, the differential slippage rates of the traps takes over, trap 2 overtaking trap 1 to get occupied (regime IV). Since trap 2 talks to trap 1 but not to the channel (recall the U_0 hierarchy), it expels the charge on trap 1, thereby unblocking the channel (regimes IV and V). As before, regime IV proceeds through an RTS sequence (characterizing the second trap), thus creating the RTS-flanked blockade window seen experimentally and theoretically.

The RTS signature was analyzed by taking high resolution scans in Regime IV corresponding to the switching of trap 2 [Fig. 3(a)]. Knowing the scan rate, we can extract information about τ_c and τ_e for trap 2, whose ratio is plotted as a

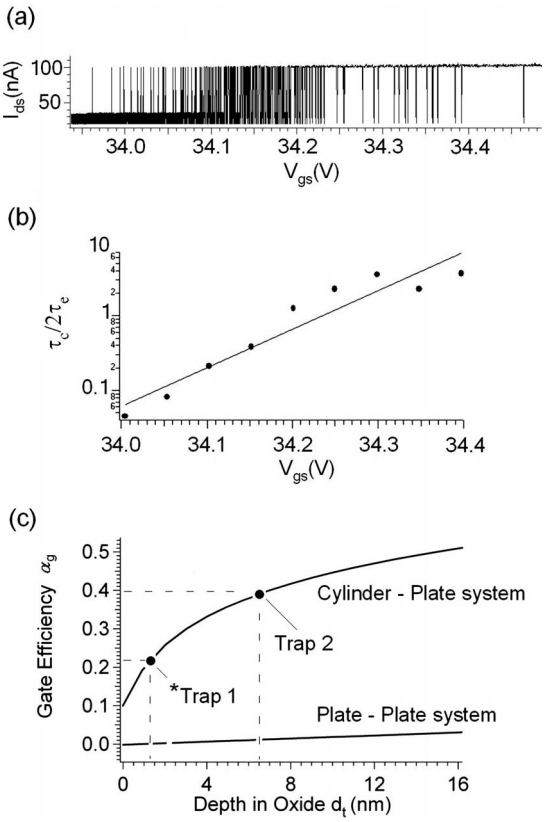

FIG. 3. (a) High-resolution gate sweep showing RTS switching. Time interval between successive data points is 2 ms (scan rate: 0.125 V/sec; resolution: 4000 data point/V). (b) Capture to emission time ratio vs V_{gs} for regime IV. (c) Extraction of trap positions, both spatial and spectral (with respect to the fermi level) from experiment and simulation.

function vs V_{gs} in Fig. 3(b). By Eq. (3), α_g is given by slope of the fitted line, which is found to be 0.40 ± 0.04. The trap energy ϵ_{T2} can be obtained from the y intercept and is found to be 5.6 ± 0.6 eV relative to the Fermi level. The high to low current switching region characterizing the first trap (regime II) is not analyzed due to lack of adequate data points.

The small operating drain bias ($\sim$0.1 V) relates the gate capacitive factor α_g directly to an effective trap depth d_t under the oxide surface. The relationship is linear in the oxide for a regular MOSFET with planar geometry, $d_t \approx \alpha_g t_{ox}$, with t_{ox} denoting the thickness of the oxide layer.[24,25] Because of the cylindrical structure of the carbon nanotube FET the potential profile across the oxide varies logarithmically with distance from the center of the conductor. The gate capacitance per unit length for a CNTFET is given by $C = 2\pi\epsilon / \ln(2h/r)$, where r is the nanotube radius, $h = t_{ox} + r$ and ϵ is the permittivity of the oxide. Using Eq. (3) and the above capacitance, trap 2 is estimated to be 6.34 nm below the CNT in the oxide, consistent with typical values in the literature ($\sim$0.2–20 nm).[25–27] Figure 3(c) shows the trap positions extracted from our simulation, assuming a logarithmically varying potential. For a linear potential, the significantly different α_gs for unblocking require one of the traps to sit too far from the CNT to influence its current. The absolute necessity for fast varying potentials underscores the importance of low dimension to see these trap correlations.

The data reveal a rich spectrum of additional defect states, such as smaller current jumps at the bottom of the blockade window, which we attribute to low-frequency device noise.[28] Furthermore, there is a gate offset V_{g0} defining the minimum in the typical ambipolar[22] CNT-FET curve. The location of this minimum is independent of V_{ds} and is shifted by 19.0 V. The observed blockade window shows an additional drift to lower gate voltage with time upon repeat scanning of V_{gs} between 35 to 25 V over 18 s intervals. The width of the window, however, remains the same between traces, so that each successive time trace can be superposed by a shift of 2 V. Thermal treatment in H_2 for 4.5 h at 200 °C followed by cooling and desiccation removes the RTS but preserves the hysteretic shift, inconsistent with Ref. 22. We tentatively attribute RTS to oxidative traps that can be passivated by H_2, while the shift in minimum V_{g0} and the hysteretic effect may be attributed to non-oxidative charge traps.

In summary, we report unique transport dynamics whereby one trap electrostatically "passivates" another without any chemical bonding between them, lifting a severe current blockade and fully restoring conduction. The rapidly varying fields around the CNT enable us to perform detailed spectroscopy with fine resolution even at room temperature [spectral and spatial data on the two traps in this Brief Report are listed in Ref. 23 and Fig. 3(c)], allowing us to envision a high precision "molecular barcode" for a wide range of surface adsorbates. Indeed, our preliminary *ab initio* simulations of RTS suggest that different molecules create different, resolvable traps in the silicon band-gap that are detectable through distinct and recoverable spectral fingerprints in the current noise.[29] Based on these observations, we suggest that it will be possible to engineer 'receptor' states along a nanotube or similar 1D channel that electrostatically couple to noncovalently bound targets for detection with ultrahigh specificity.

The authors are particularly grateful to Chong Hu for experimental assistance and to Lloyd Harriott, John Bean, and Kamil Walczak for useful discussions. This work was partially supported by the NSF NIRT and CAREER grants.

*Corresponding author; kwilliams@virginia.edu

[1] M. J. Kirton and M. J. Uren, Adv. Phys. **38**, 367 (1989).
[2] E. S. Snow, J. P. Novak, M. D. Lay, and F. K. Perkins, Appl. Phys. Lett. **85**, 4172 (2004).
[3] Fei Liu *et al.*, Appl. Phys. Lett. **86**, 163102 (2005).
[4] F. Liu, K. L. Wang, C. Li, and C. Zhou, IEEE Trans. Nanotechnol. **5**, 441 (2006).
[5] J. F. Zhang *et al.*, J. Appl. Phys. **90**, 1911 (2001).
[6] B. Kaczer, Z. Meng, and J. P. Pelz, Phys. Rev. Lett. **77**, 91 (1996).
[7] N. P. Wang, S. Heinze, and J. Tersoff, Nano Lett. **7**, 910 (2007).
[8] F. Liu, M. Bao, and K. L. Wang, Nano Lett. **5**, 1333 (2005).
[9] H. B. Peng, M. E. Hughes, and J. A. Golovchenko, Appl. Phys. Lett. **89**, 243502 (2006).
[10] F. Liu *et al.*, Phys. Rev. B **74**, 035438 (2006).
[11] Jing Kong *et al.*, Nature (London) **395**, 878 (1998).
[12] Y. Zhang *et al.*, Science **285**, 1719 (1999).
[13] R. Martel *et al.*, Phys. Rev. Lett. **87**, 256805 (2001).
[14] F. Liu and K. L. Wang, Nano Lett. **8**, 147 (2008).
[15] S. Datta, *Quantum Transport: Atom to Transistor* (Cambridge University Press, Cambridge, 2005).
[16] S. Vasudevan, K. Walcak, and A. W. Ghosh, IEEE Sens. J. **8**, 857 (2008).
[17] J. Guo, Ph.D. thesis, The University of Melbourne, 2006.
[18] K. S. Ralls *et al.*, Phys. Rev. Lett. **52**, 228 (1984).
[19] D. H. Cobden and M. J. Uren, Microelectron. Eng. **22**, 163 (1993).
[20] M. Xiao, I. Martin, E. Yablonovitch, and H. W. Jiang, Nature (London) **430**, 435 (2004).
[21] M. Xiao, I. Martin, and H. W. Jiang, Phys. Rev. Lett. **91**, 078301 (2003).
[22] Woong Kim *et al.*, Nano Lett. **3**, 193 (2003).
[23] The energy level positions used in the plots are $\epsilon_{ch}=1$ meV, $\epsilon_{T1}=3$ eV, and $\epsilon_{T2}=5.6$ eV relative to E_F. Broadenings $\gamma_{S,ch} = \gamma_{D,ch} = \gamma_{S,T1} = \gamma_{D,T1} = \gamma_{S,T2} = \gamma_{D,T2} = 50$ meV. Charging energies $U_{0,T1-ch}=0.2$ eV, $U_{0,T1-T2}=0.48$ eV, and $U_{0,T2-ch}=0$ eV.
[24] N. V. Amarasinghe, Z. Çelik-Butler, A. Zlotnicka, and F. Wang, Solid-State Electron. **47**, 1443 (2003).
[25] N. V. Amarasinghe, Z. Çelik-Butler, and P. Vasina, Microelectron. Reliab. **40**, 1875 (2000).
[26] P. G. Collins, M. S. Arnold, and Ph. Avouris, Science **292**, 706 (2001).
[27] F. Liu, K. L. Wang, D. Zhang, and C. Zhou, Appl. Phys. Lett. **89**, 243101 (2006).
[28] J. S. Kolhatkar *et al.*, *European Solid-State Device Research (ESSDERC) '03. 33rd Conference*, 16–18 Sept. 2003, pp. 549–552.
[29] S. Vasudevan and A. W. Ghosh (unpublished).